Turkish Journal of Electrical Engineering & Computer Sciences

http://journals.tubitak.gov.tr/elektrik/

Research Article

Turk J Elec Eng & Comp Sci
(2013) 21: 330 – 349
© TÜBİTAK
doi:10.3906/elk-1107-35

Characterization of internal disturbances and external faults in transformers using an S-transform–based algorithm

Abdolaziz ASHRAFIAN[1,*], **Mehrdad ROSTAMI**[1], **Gevork B. GHAREHPETIAN**[2]
[1]Department of Engineering, Shahed University, Tehran, Iran
[2]Electrical Engineering Department, Amirkabir University of Technology, Tehran, Iran

Received: 19.07.2011 • **Accepted:** 14.11.2011 • **Published Online:** 22.03.2013 • **Printed:** 22.04.2013

Abstract: In this paper, the S-transform is used to discriminate between the internal disturbances and external faults of transformers. The proposed algorithm consists of 2 stages. The internal disturbances and the external faults are distinguished in the first stage. Next, the S-transform is applied to differential currents of faulty phases and the absolute deviation of the S-matrix is calculated. The relay scheme issues a trip signal in the case of an internal fault, according to the absolute deviation of the S-matrix. The scheme is implemented in a MATLAB environment and the inputs are differential currents, derived from EMTP software. In order to simulate the internal turn-to-turn and turn-to-earth faults, the power transformer is modeled using 8 × 8 RL matrices, obtained from the subroutine BCTRAN of the EMTP software. The differential current signals are contaminated by noise and the robustness of the algorithm in a noisy environment is investigated. The performance of the S-transform and the wavelet transform are compared. It is shown that the proposed algorithm is superior to wavelet transform-based methods.

Key words: Transformer, S-transform, inrush current, internal fault, external fault

1. Introduction

The transformer differential protection has been proposed for detecting internal faults in transformers. The most important problem with the differential protection is the discrimination of internal faults from magnetizing inrush current and external faults, which can result in the saturation of current transformers (CTs). Several methods have been proposed to detect them. For example, a modal analysis method was suggested in [1]. The magnetizing inrush current has a larger amount of the second-order harmonic component in comparison with the internal faults. Some of the conventional transformer protection techniques employ the second-order harmonic to identify the inrush current [2–4]. However, the second-order harmonic may exist in some internal faults, due to CT saturation, nonlinear fault resistance, or the use of extra-high-voltage underground cables or capacitors, as well as the capacitance of a long under-load or no-load transmission line to which the transformer is connected. In addition, the second-order harmonic component in the magnetizing inrush currents tends to be relatively small in modern large power transformers because of advances in transformer design and construction and improvements in power transformer core materials [5]. In [6] and [7], wavelet packet-based methods were proposed. The method suggested in [7] requires the measurement of both the voltage and current signals; hence, a large computational burden is required. Discrete wavelet transform (DWT)-based algorithms for discriminating between the magnetizing inrush current and short circuit current were suggested in [8] and

*Correspondence: az.ashrafian@gmail.com

[9]. Moreover, protective methods have been proposed using a combination of DWT and fuzzy logic [10,11], neural networks [5,12], Gaussian mixture model [13], correlation factor [14], and support vector machine [15,16]. However, DWT-based methods are easily influenced by noise [17]. Moreover, the frequency characteristics of DWT decomposition filters are not ideal and suffer leakage, where the analyzed signal frequency is close to the edge of the frequency band of the filters [17]. Since the S-transform is less influenced by noise, some S-transform–based schemes were suggested for overcoming the noise problems in [17–22]. In previous works, turn-to-turn and turn-to-earth faults as well as external faults considering CT saturation have not been studied.

In this paper, an S-transform–based algorithm is suggested for discriminating among the external faults, inrush currents, internal turn-to-turn and turn-to-earth faults, and internal faults during transformer energization. In order to detect the external faults and the CT's saturation and ratio mismatch, the proposed algorithm is implemented in 2 stages, fault detection and fault discrimination. In the suggested algorithm, the S-transform is applied to differential currents of the faulty phases and the absolute deviation of the S-matrix is calculated. Next, the absolute deviation of the S-matrix is used to discriminate between the fault and inrush currents. In order to compare the performance of the S-transform, a wavelet-based method is implemented and the results are compared with the proposed algorithm results in a noisy environment.

2. S-transform

Assume that $x(t)$ is a time-varying signal, and then the continuous wavelet transform (CWT) is given by the following equation:

$$CWT(\tau,a)=\int_{-\infty}^{+\infty}x(t)w(\tau-t,a)dt, \tag{1}$$

where τ and a are the translating and scaling parameters, respectively, and $w(t)$ is the wavelet function. The S-transform of the signal given by Stockwell et al. [23] is as follows:

$$S(\tau,f)=\int_{-\infty}^{+\infty}x(t)\left[\frac{|f|}{\sqrt{2\pi}}\times\exp\left(\frac{-f^2(\tau-t)^2}{2}\right)\times\exp(-2\pi ift)\right]dt, \tag{2}$$

where S denotes the S-transform of $x(t)$, which are time-varying signals; f denotes the frequency; and τ is a parameter that controls the position of the Gaussian window on the t-axis. Next, the S-transform of function $x(t)$ can be defined as a CWT with a particular wavelet multiplied by an additional term, which is a phase factor:

$$S(\tau,f)=CWT(\tau,a)\exp(-2\pi ft) \tag{3}$$

However, the S-transform is not strictly a wavelet transform [23]. The generalized S-transform can be defined from the original S-transform by replacing the Gaussian window with a generalized window, as follows [20]:

$$S(\tau,f,p)=\int_{-\infty}^{+\infty}x(t)w_{gen}(\tau-t,f,p)\exp(-2\pi ift)dt \tag{4}$$

where p denotes a set of parameters that control the shape of the generalized window. The hyperbolic S-transform (HST) is obtained from the generalized S-transform by replacing the generalized window with a

hyperbolic window, as follows:

$$w_{hyp} = \frac{2\,|f|}{\sqrt{2\pi}(\gamma_f + \gamma_b)} \times \exp\left[\frac{-f^2\left[U(\tau - t, \left\{\gamma_f, \gamma_b, \lambda_{hyp}^2\right\})\right]^2}{2}\right] \tag{5}$$

where

$$U(\tau - t, \{\gamma_f, \gamma_b, \lambda_{hyp}^2\}) = \left[\frac{\gamma_f + \gamma_b}{2\gamma_f\gamma_b}\right](\tau - t - \zeta) + \left[\frac{\gamma_f - \gamma_b}{2\gamma_f\gamma_b}\right]\sqrt{(\tau - t - \zeta)^2 + \lambda_{hyp}^2} \tag{6}$$

Here, γ_f and γ_b are the forward-taper and backward-taper parameters, respectively, and λ_{hyp} is the positive curvature parameter. U is a hyperbola in $(\tau - t)$ and its shape is defined by the above mentioned parameters. ζ is defined as follows:

$$\zeta = \sqrt{\frac{(\gamma_f - \gamma_b)^2\lambda_{hyp}^2}{4\gamma_f\gamma_b}} \tag{7}$$

The translation by ζ ensures that the peak of $\mathrm{w_{hyp}}$ occurs at $\tau - t = 0$. The S-transform windows must satisfy Eq. (8):

$$\int_{-\infty}^{+\infty} w(\tau - t, f, p)d\tau = 1 \tag{8}$$

It is easy to show that the averaging of the S-transform over all of the values of τ is the Fourier transform of $x(t)$ and that there is a joint between the S-transform and the Fourier transform.

$$\int_{-\infty}^{+\infty} S(\tau, f, p)d\tau = \int_{-\infty}^{+\infty} x(t)\exp(-2\pi ift)\times$$

$$\int_{-\infty}^{+\infty} w(\tau - t, f, p)d\tau dt = \int_{-\infty}^{+\infty} x(t)\exp(-2\pi ift)dt = X(f) \tag{9}$$

The discrete version of the HST can be defined as follows [18]:

$$S[n, j] = \sum_{m=0}^{N-1} X(m + n)G(m, n)exp(i2\pi mj), \tag{10}$$

where N is the total number of samples and n, m, and j vary from 0 to *N-1*. G(m,n) and $X(m + n)$ are the Fourier transforms of the hyperbolic window and the frequency-shifted discrete Fourier transform $X[m]$, respectively. They are given by the following equations:

$$G(m, n) = \frac{2f}{\sqrt{2\pi}(\gamma_f + \gamma_b)}\exp(\frac{-f^2U^2}{2n^2}), \tag{11}$$

where

$$U = \left[\frac{\gamma_f + \gamma_b}{2\gamma_f\gamma_b}\right](t) + \left[\frac{\gamma_f - \gamma_b}{2\gamma_f\gamma_b}\right]\sqrt{t^2 + \lambda_{hyp}}, \tag{12}$$

and

$$X(m) = \frac{1}{N} \sum_{m=0}^{N-1} x(k) \exp(-i2\pi nk). \tag{13}$$

If 2 windows have the same width in the time domain, a symmetrical window provides better frequency resolution than an asymmetrical window. Therefore, at high frequencies, where the window is narrow and the time resolution is good and less critical, the shape of the window converges toward the Gaussian window (i.e. a symmetrical window). However, at low frequencies, where the window is wide and the frequency resolution is less critical, an asymmetrical window can be used (e.g., a hyperbolic window). Therefore, the S-transform with a frequency-dependent shaped window is used in this paper.

3. Proposed algorithm

The proposed algorithm consists of 2 stages, the detection and the discrimination stages. If a disturbance is recognized as an internal disturbance in the detection stage, the HST will be applied to the differential current signal. The output of the HST is an $M \times N$ matrix, named the S-matrix, with samples of the analyzed signal (time) in columns and frequency in rows. Next, the sum of the absolute deviation (SAD) of the S-matrix for the decomposed signal is calculated. The suggested algorithm discriminates between the internal faults and the inrush currents using the SAD.

3.1. Disturbance detection stage

Small differential currents can exist in normal operation mode due to the CT's ratio mismatch, accuracy differences, saturation in the case of external faults, or abrupt tap changes. In order to prevent maloperation caused by the mentioned problems, a detection stage should be considered. Percentage differential relay provides a solution to these problems, and so a threshold current value ($i_{\lim}$) should be used. If the differential current exceeds this value, it will be recognized as an internal disturbance (i.e. internal fault or inrush current) [24]. This value is defined as follows:

$$i_{\lim} = k.\frac{(i_{\sec CT} + i_{perCT})}{2} \tag{14}$$

where i_{perCT} and $i_{\sec CT}$ are the currents of primary and secondary CTs, respectively, and k is the slope of the differential relay characteristic. The lower values of k can provide more sensitive protection and can have values such as 0.1, 0.2, or 0.4 [25].

3.2. Disturbance discrimination stage

In the disturbance discrimination stage, the S-transform is applied to the differential currents of the faulty phases and the absolute values of the S-matrix, $M \times N$ matrices with complex values, are defined. Next, the median of each column is computed. The result will be a $1 \times N$ vector, named the median vector, whose ith element is the median of the ith column of the S-matrix. Now, the absolute difference of each element of the ith column of the S-matrix from its median can be determined. The sum of the absolute differences of the column i is the ith element of the $1 \times N$ vector, named the absolute deviation vector (ADV). The sum of all of the ADV elements, named SAD, can be computed as follows:

$$Median\ Vector\,(1 \times N) = Median\ [abs(\text{S-matrix})] \tag{15}$$

$$ADV(1,n) = \sum_{n=1}^{N} \sum_{m=1}^{M} abs[absS(m,n) - Median\ Vector(1,n)], \tag{16}$$

$$SAD = \sum_{n=1}^{N} ADV(1,n), \tag{17}$$

where N and M are the number of rows and columns of the S-matrix, respectively (i.e. sample and frequency, respectively). The simulation results show that the SAD has high values in the case of internal faults, while it has lower values during inrush currents. Hence, it is easy to discriminate between inrush currents and internal faults using the SAD values. A flowchart of the suggested algorithm is presented in Figure 1. The SAD can be computed for a data set that may not have a mean or variance [9]. For the calculation of the standard deviation, the distances from the mean value are squared and large deviations are multiplied by higher coefficients [9]. However, the SAD is a more effective index than the variance and standard deviation, which were used in [17–19] to discriminate between inrush and fault currents.

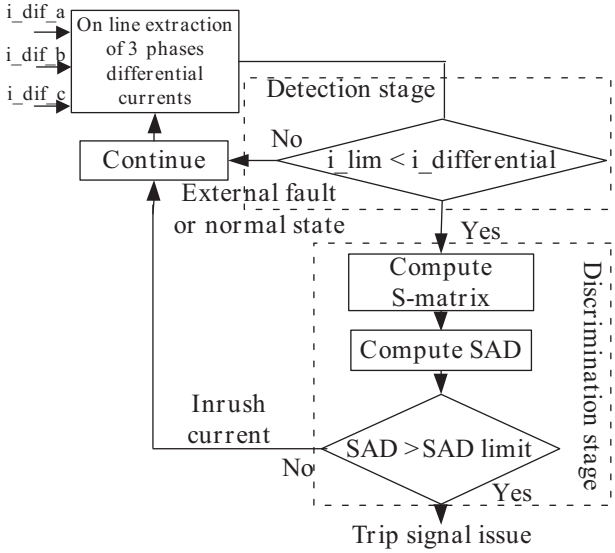

Figure 1. Flowchart of the proposed algorithm.

4. Modeled system

The power system shown in Figure 2 has been simulated by EMTP software. The proposed algorithm is implemented in a MATLAB environment and the inputs are differential currents derived from the EMTP software. The transmission lines have been modeled by π sections. The simulated transformer is a 31.5 MVA, 132/33 kV Yg/D connected transformer. The primary winding has 980 turns wound in 10 layers and the secondary winding has 424 turns wound in 4 layers. The details can be found in [26].

4.1. Transformer winding model for the internal faults

In order to simulate turn-to-earth and turn-to-turn faults, it is necessary to divide the transformer winding into 2 and 3 subcoils, respectively. If a transformer terminal model is known in terms of the winding resistance and the self and mutual inductances, 6 $\times$ 6 RL matrices from the BCTRAN routine that is available in the

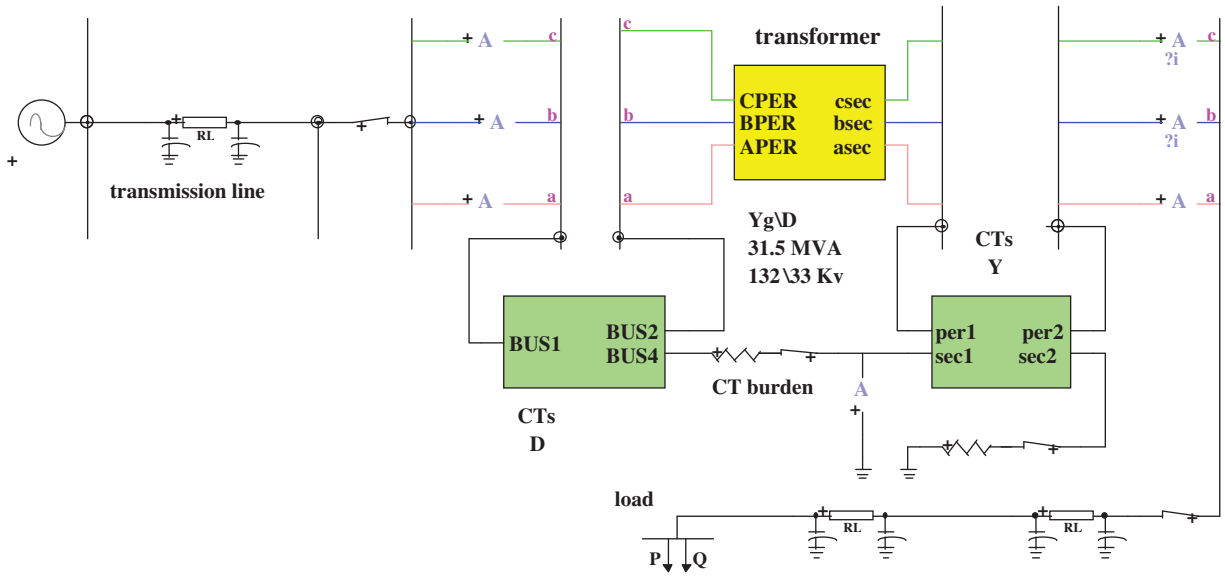

Figure 2. Simulated power system.

EMTP software can be formed for a transformer. Using these 6 × 6 RL matrices, new 7 × 7 and 8 × 8 RL matrices can be computed for the turn-to-earth and turn-to-turn faults, respectively [27,28]. In order to study the turn-to-earth and turn-to-turn faults, phase B of the primary winding is divided into 3 parts, as shown in Figure 3 (these parts have 637, 49, and 294 turns). Therefore, the power transformer has been modeled using the linear 8 × 8 RL matrices, as follows:

$$R = \begin{bmatrix} R_1 & 0 & 0 & 0 & 0 & 0 & 0 & 0 \\ 0 & R_2 & 0 & 0 & 0 & 0 & 0 & 0 \\ 0 & 0 & R_a & 0 & 0 & 0 & 0 & 0 \\ 0 & 0 & 0 & R_b & 0 & 0 & 0 & 0 \\ 0 & 0 & 0 & 0 & R_c & 0 & 0 & 0 \\ 0 & 0 & 0 & 0 & 0 & R_4 & 0 & 0 \\ 0 & 0 & 0 & 0 & 0 & 0 & R_5 & 0 \\ 0 & 0 & 0 & 0 & 0 & 0 & 0 & R_6 \end{bmatrix} \tag{18}$$

$$L = \begin{bmatrix} L_1 & M_{12} & M_{1a} & M_{1b} & M_{1c} & M_{14} & M_{15} & M_{16} \\ M_{21} & L_2 & M_{2a} & M_{2b} & M_{2c} & M_{24} & M_{25} & M_{26} \\ M_{a1} & M_{a2} & L_a & M_{ab} & M_{ac} & M_{a4} & M_{a5} & M_{a6} \\ M_{b1} & M_{b2} & M_{ba} & L_b & M_{bc} & M_{b4} & M_{b5} & M_{b6} \\ M_{c1} & M_{c2} & M_{ca} & M_{cb} & L_c & M_{c4} & M_{c5} & M_{c6} \\ M_{41} & M_{42} & M_{4a} & M_{4b} & M_{4c} & L_4 & M_{45} & M_{46} \\ M_{51} & M_{52} & M_{5a} & M_{5b} & M_{5c} & M_{54} & L_5 & M_{56} \\ M_{61} & M_{62} & M_{6a} & M_{6b} & M_{6c} & M_{64} & M_{65} & L_6 \end{bmatrix} \tag{19}$$

where R_n and L_n are the resistance and the self-inductance of the nth coil, and M_{nm} is the mutual inductance between the nth and mth coils. R_a, R_b, R_c and L_a, L_b, L_c are the resistance and the self-inductance of the faulty coil, which is divided into 3 parts: a, b, and c. (i.e. phase B of the primary winding, shown in

Figure 3). The saturation effects are taken into account through the nonlinear hysteretic reactors, placed across the terminals of the secondary windings. Small shunt capacitances are connected across the windings to model the high-frequency capacitive behavior of the transformer.

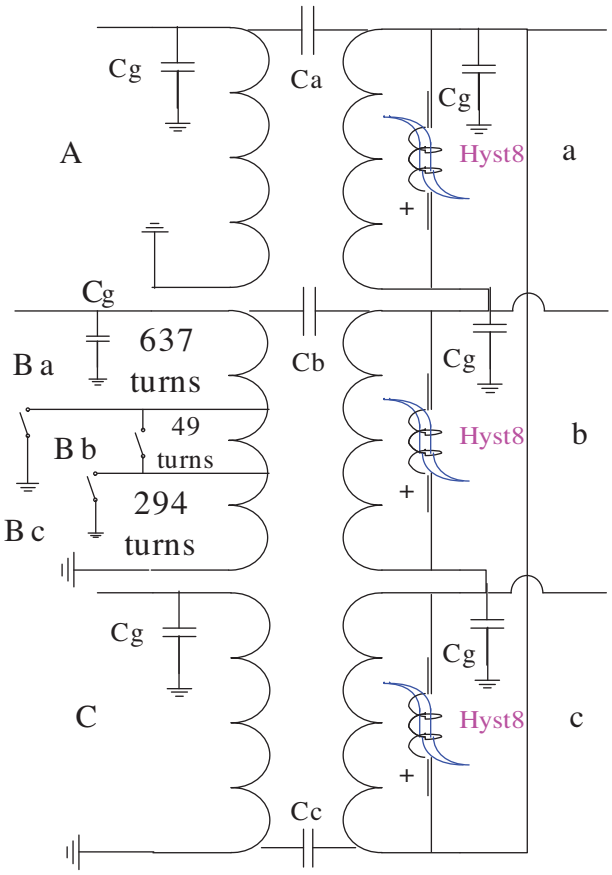

Figure 3. Transformer windings model.

4.2. Current transformer model

The differential protection system requires precise representation of the CT model. The CTs have been modeled as presented in [29–31]. The subroutines HYSTERESIS and SATURATION in EMTP have been used to simulate the CTs' characteristics. A nonideal transformer coupled with a nonlinear hysteretic reactor has been used for modeling the CTs, as shown in Figure 4. The CTs are connected in Δ and Y on the primary and secondary sides of the power transformer, respectively. The saturation characteristic of the secondary CTs, which are 1200-5A, is illustrated in Figure 5.

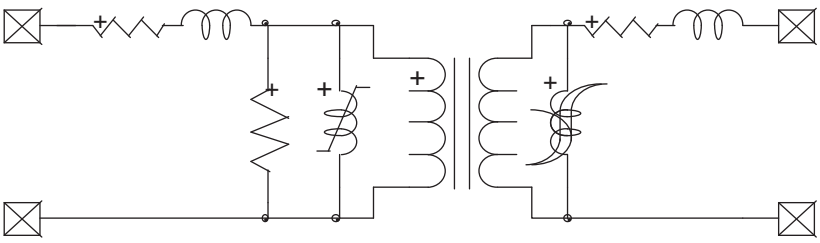

Figure 4. Current transformer model.

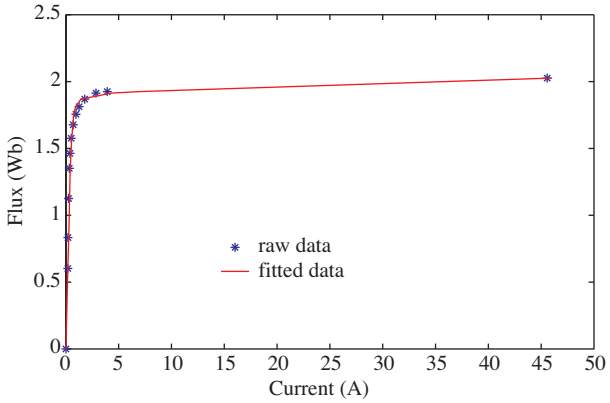

Figure 5. Saturation characteristics of secondary CTs.

5. Simulation results and discussion

Data for various operating conditions such as inrush current, external fault, and internal faults have been generated using the simulated model shown in Figure 2. Moreover, the internal turn-to-turn and turn-to-earth faults, the energizing of the transformer with the internal fault, and the CT's saturation during the external faults have been studied. A sampling rate of 5 kHz is chosen (i.e. 100 samples per fundamental frequency cycle based on 50 Hz). The S-transform is employed and the differential currents are analyzed. Next, the absolute deviation vector and the SAD for the S-matrix are calculated. Typical differential currents, time–

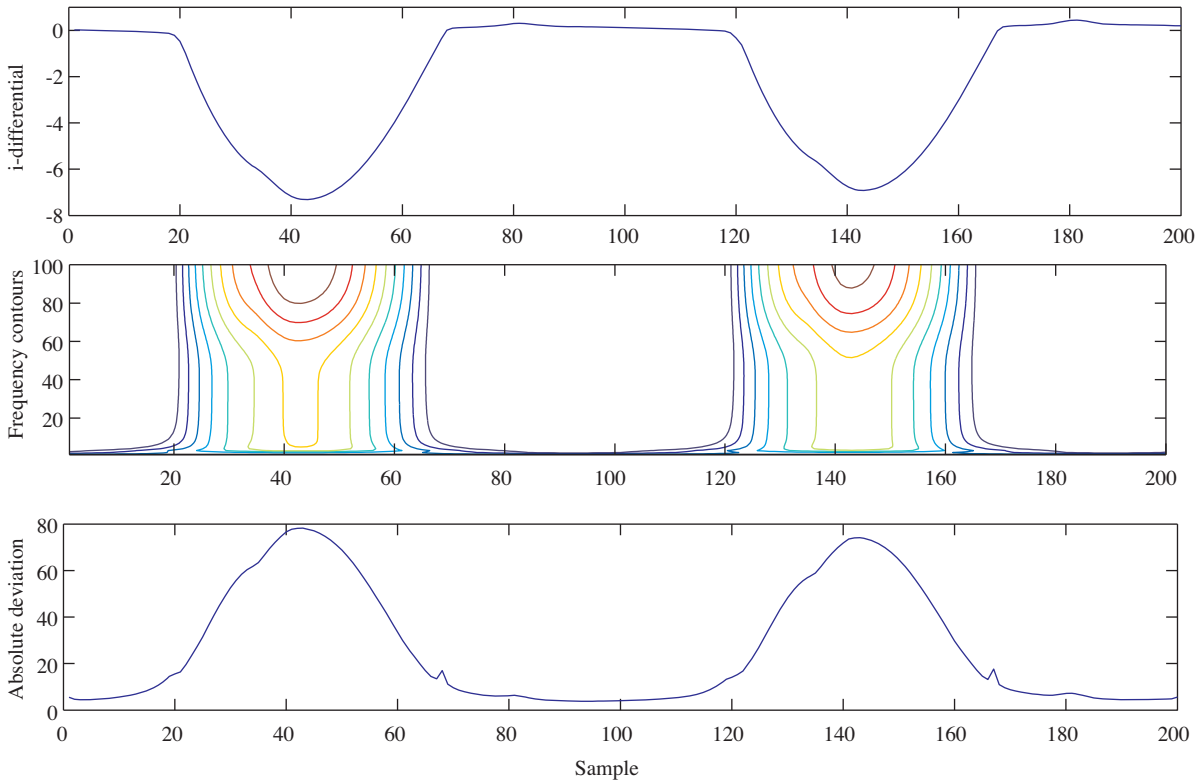

Figure 6. Differential current, S-contours, and ADV for inrush current.

frequency contours for the S-matrix, and the ADV are illustrated in Figures 6–11. The differential current, time–frequency contours, and ADV for an inrush current are presented in Figure 6. It is found that the ADV values and time–frequency contours have been interrupted and there is a consistent time interval between them. The ADV values are close to 0 at the interrupted intervals. Figure 7 shows the differential current and time–frequency contours as well as the absolute deviations for an internal turn-to-earth fault at turn 294 of phase B in the primary winding. Figure 8 illustrates the time–frequency contours and absolute deviation during the transformer energizing while a turn-to-turn fault occurs between turns 294 and 343 of phase B in primary winding. The time–frequency contours and ADV values for an internal fault in the transformer terminals are shown in Figure 9. It is clear that unlike the inrush current, the contours and ADV values are extended during the fault noninterruptedly and continuously. Moreover, the ADV values are not close to 0 during the faults. Figure 10 depicts the time–frequency contours and ADV values for a case where a turn-to-turn fault occurs between turns 294 and 343 of phase B. It can be seen that contours are presented continuously and the ADV values have high amplitude. Hence, contour behavior and ADV values in turn-to-turn faults are similar to other faulty cases. Figure 11 shows the differential currents of phase b and c for an external bcg fault (i.e. the fault of phase b and c of the secondary side to the ground) in the middle of the transmission line, where capital and lowercase letters represent the primary and secondary windings, respectively. As is clear, the CTs have been saturated but the detection step recognizes this as an external fault and the discrimination stage has not been performed.

In order to investigate the performance of the proposed algorithm in noisy environments, random noise with a signal-to-noise ratio (SNR) of up to 20 dB has been added to the differential current signals. The

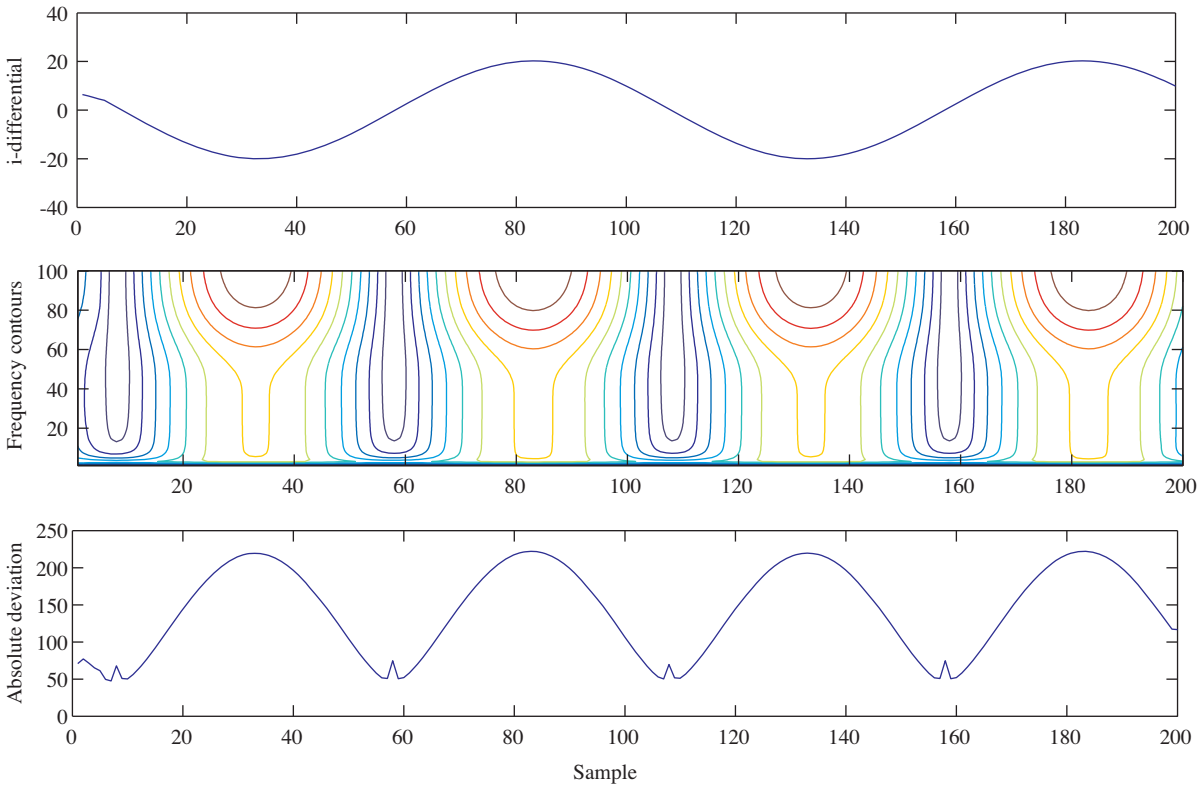

Figure 7. Differential current, S-countours, and ADV for internal turn-to-earth fault at turn 294.

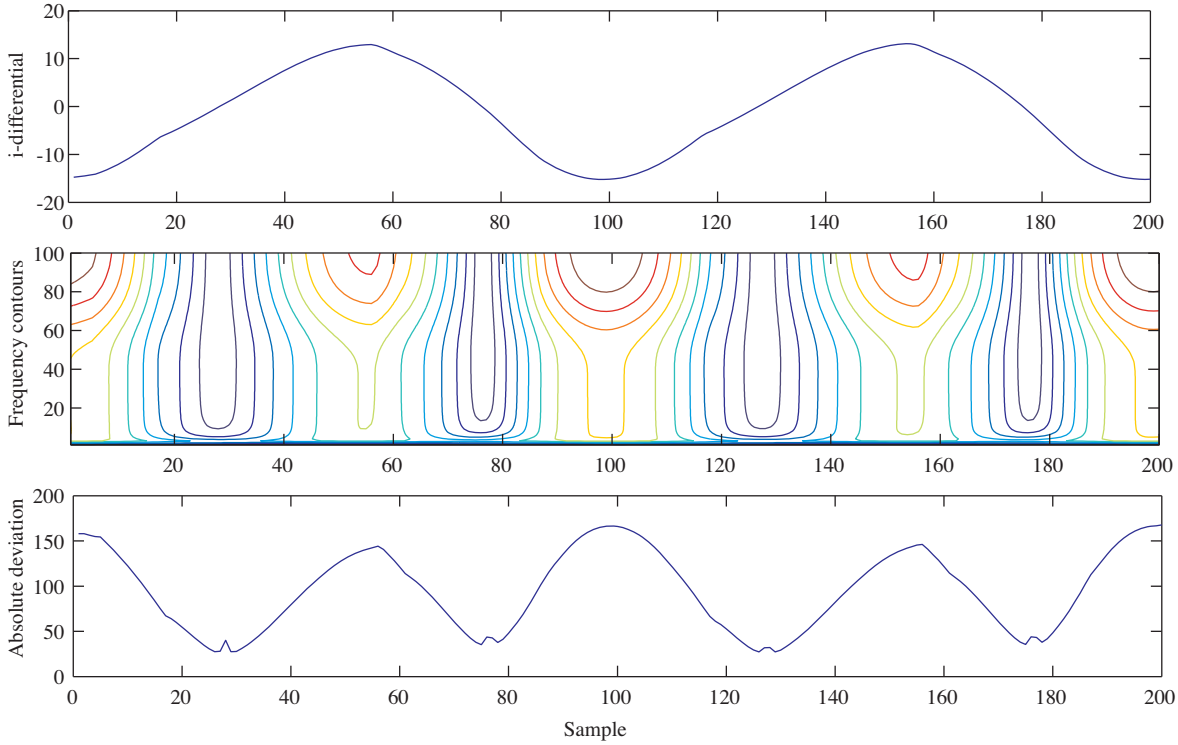

Figure 8. Differential current, S-contours, and ADV of transformer energizing for internal turn-to-turn fault between turns 294 and 343.

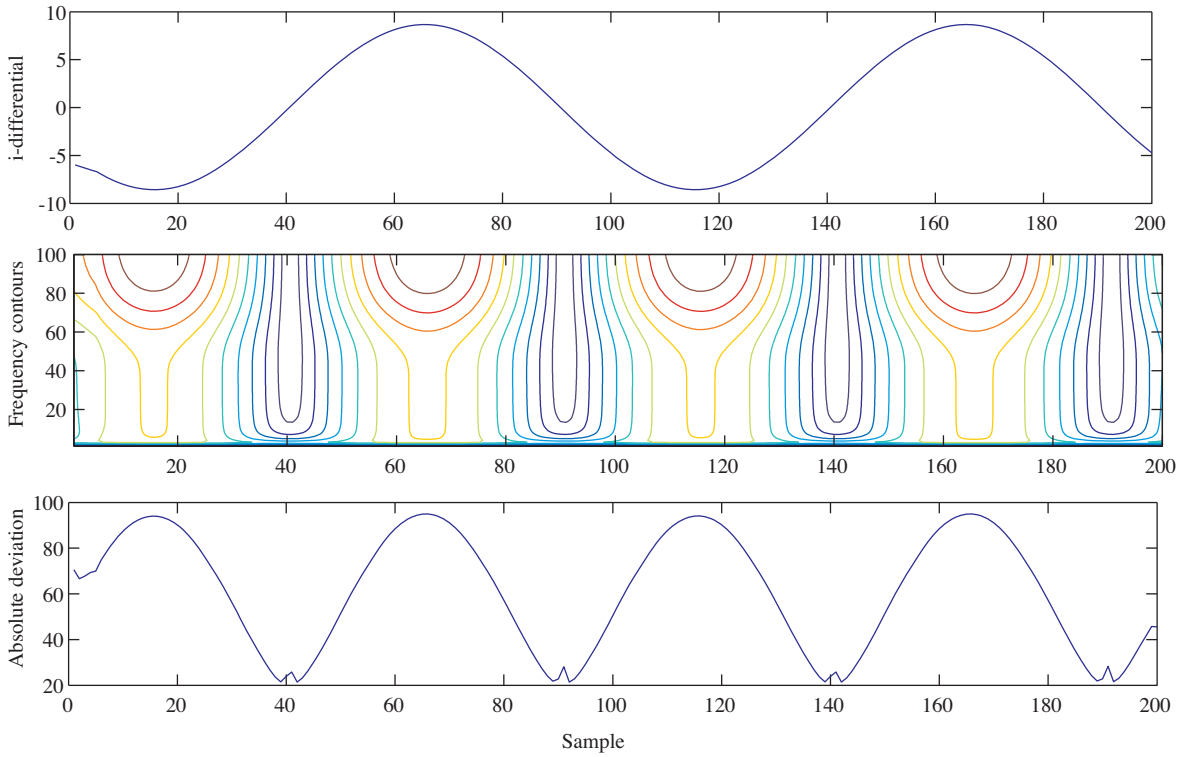

Figure 9. Differential current, S-contours, and ADV for a and c phases to ground fault in the transformer terminals.

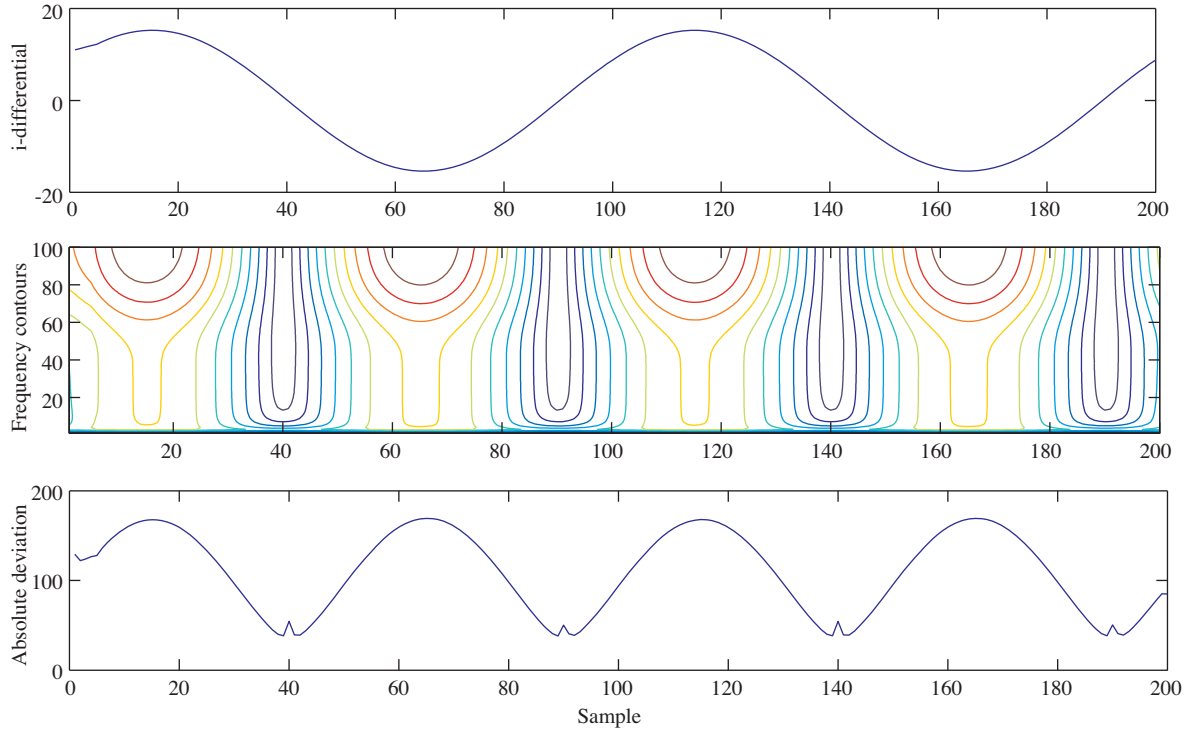

Figure 10. Differential current, S-contours, and ADV for internal turn-to-turn fault between turns 294 and 343.

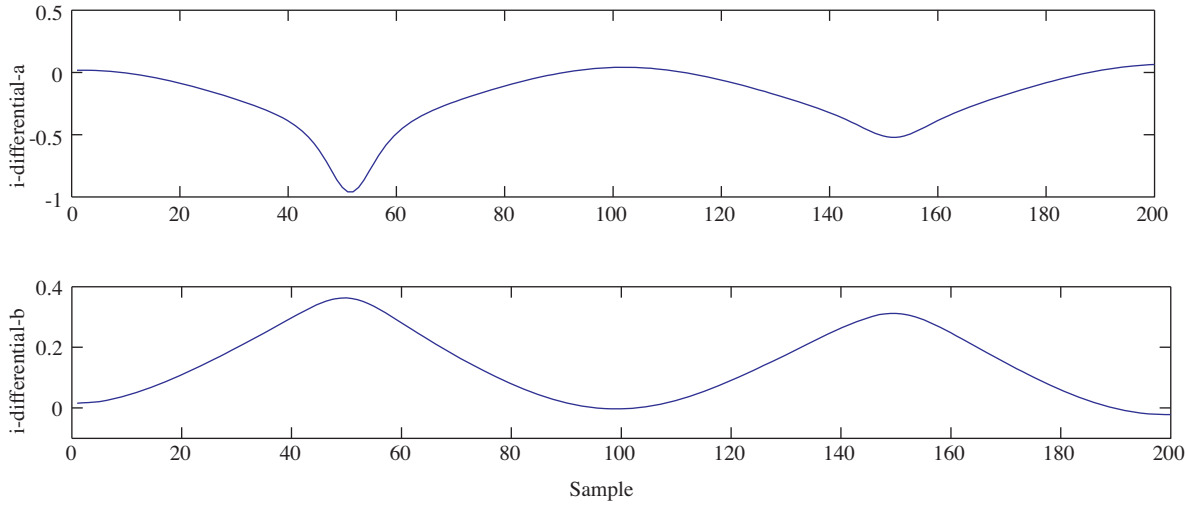

Figure 11. Differential current for external a and b phases to ground fault in middle of tranmission line; secondary CTs have been saturated.

results are shown in Figures 12–17. These cases are the same as those shown in Figures 6–11, but they are noise-contaminated. It can be seen that the ADV has not been influenced and the proposed algorithm performs robustly against the applied noise.

Various types of internal faults including different resistances, fault angles, and transformer energizing with different switching angles have been simulated. The SAD values for the S-matrix of the differential current signals have been calculated. The results for important cases are given in the Table, where Bg, acg, and ac

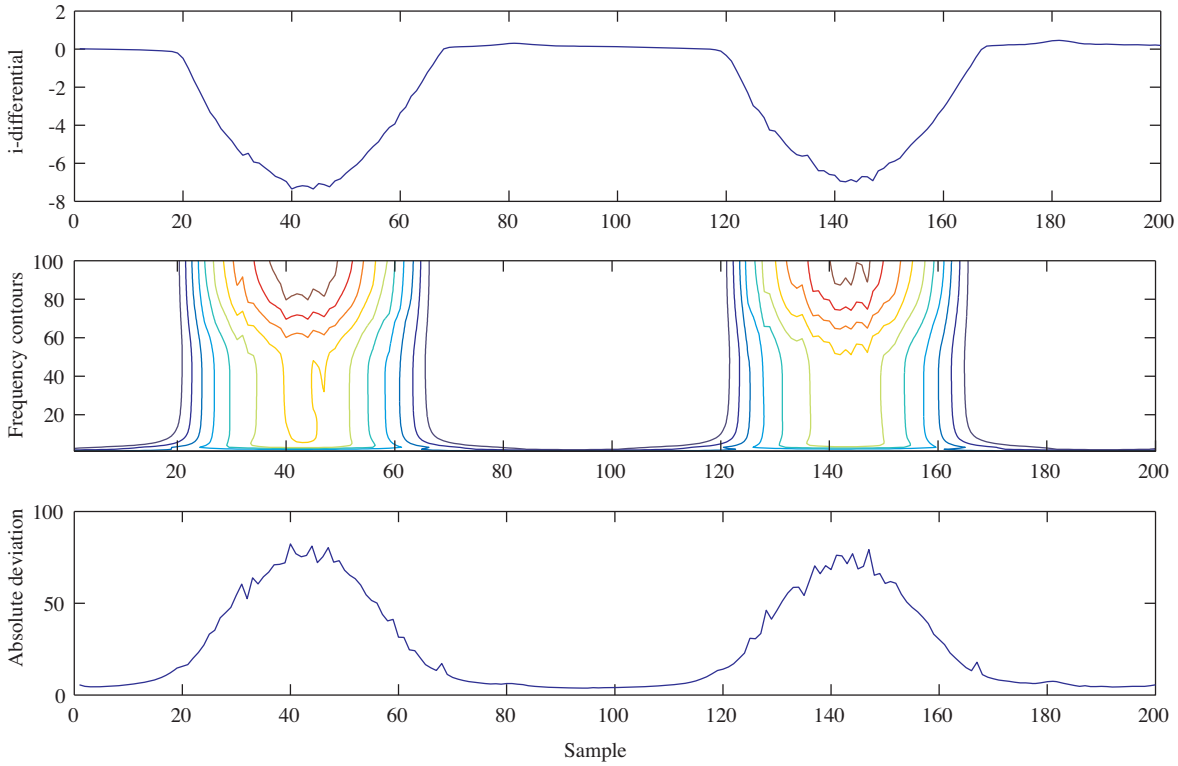

Figure 12. Differential current with SNR = 20 dB, S-contours, and ADV for inrush current.

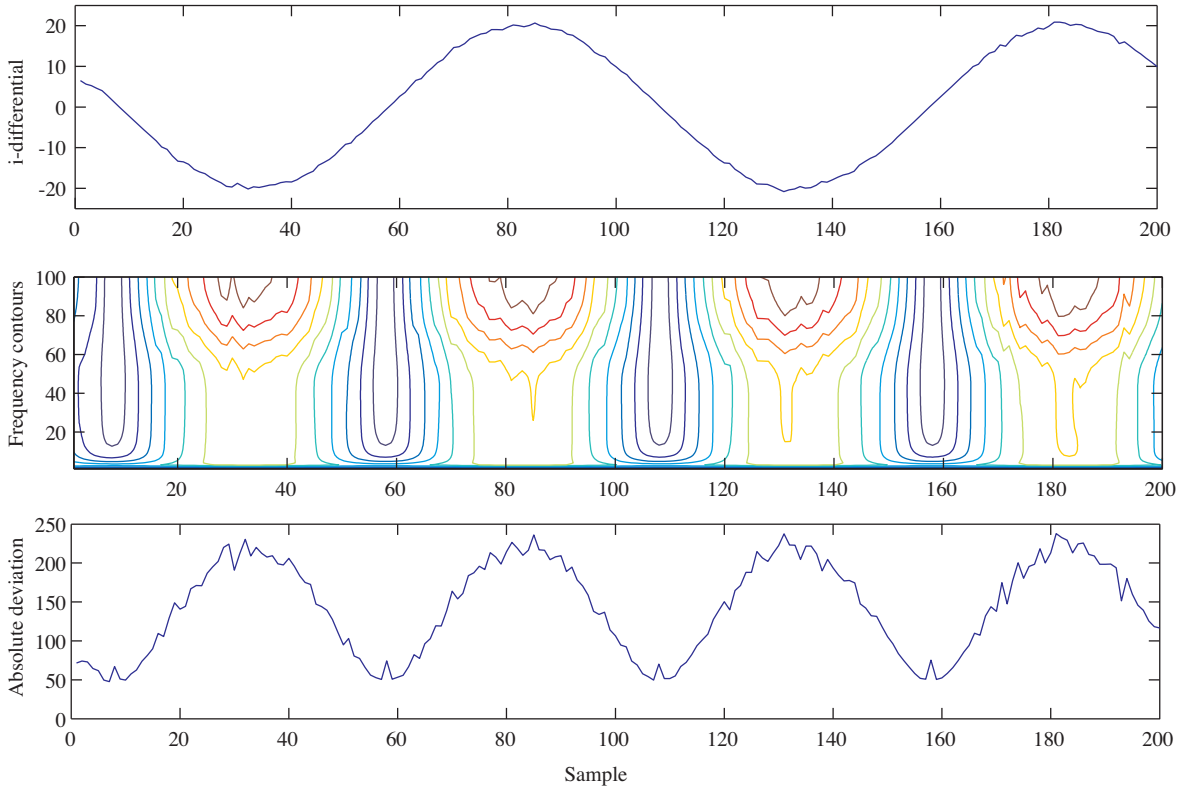

Figure 13. Differential current with SNR = 20 dB, S-contours, and ADV for internal turn-to-earth fault at turn 294.

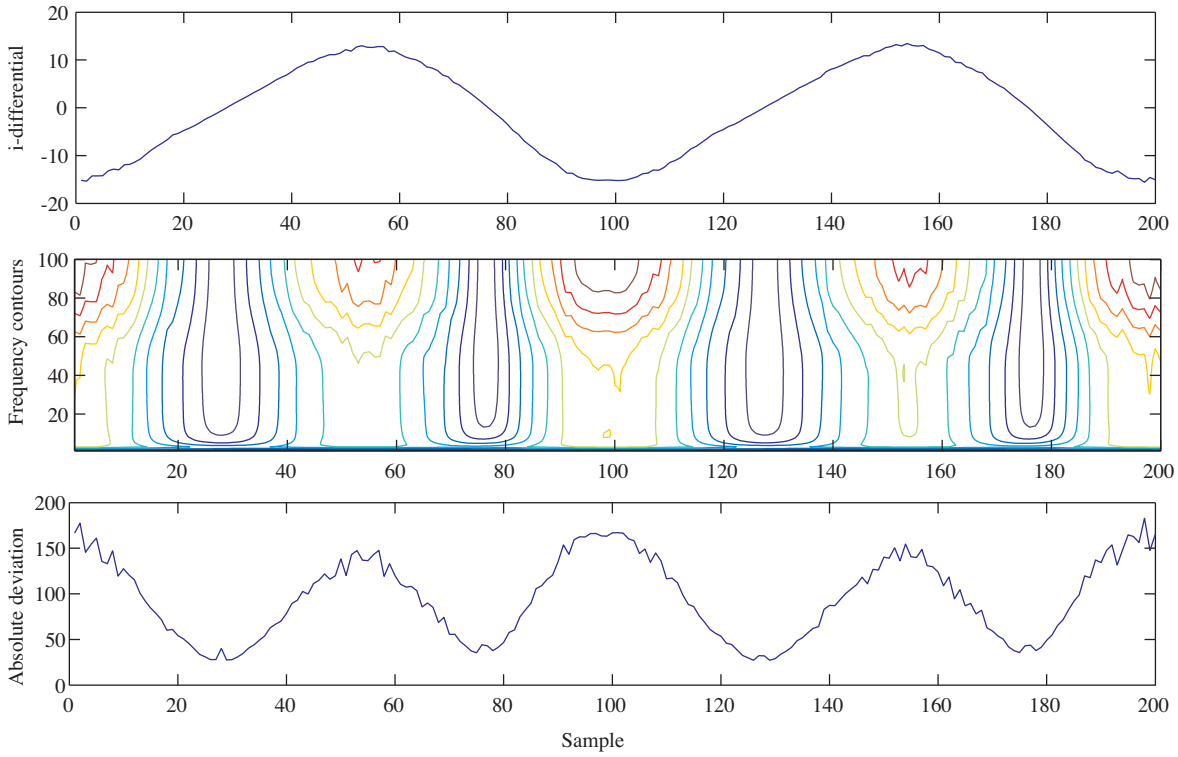

Figure 14. Differntial current with SNR = 20 dB, S-contours, and ADV for transformer energizing with internal turn-to-turn fault between turns 294 and 343.

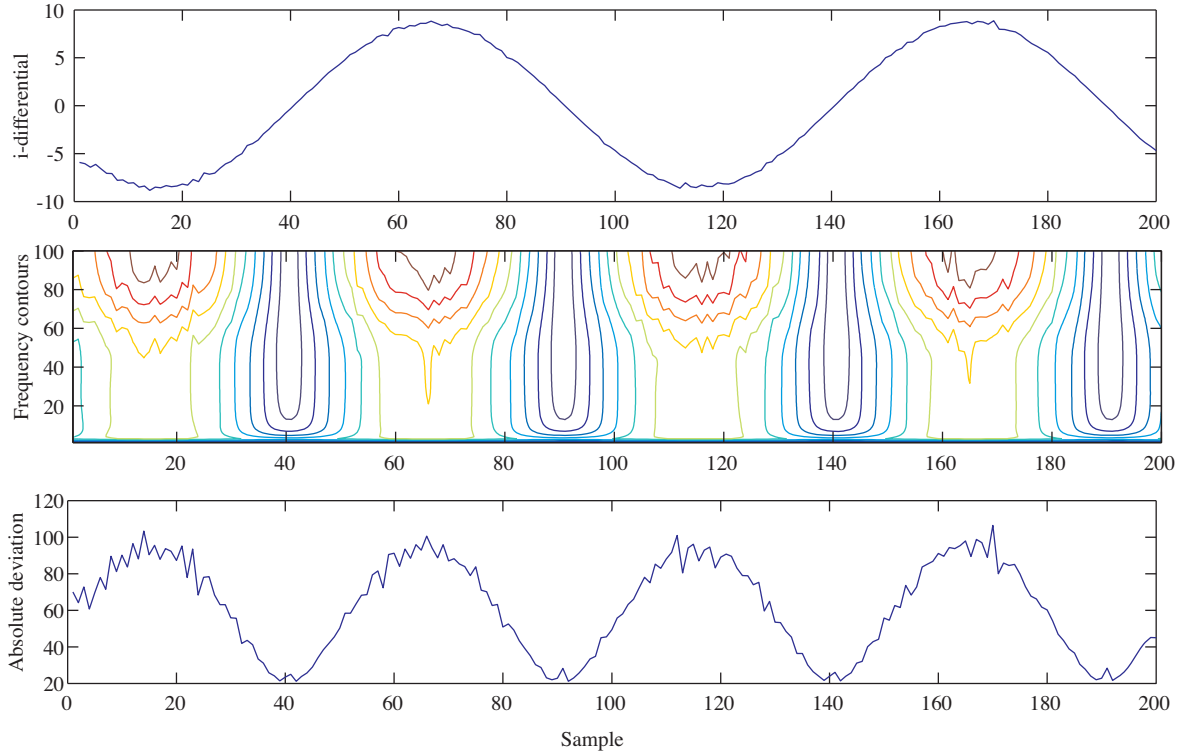

Figure 15. Differntial current with SNR = 20 dB, S-contours, and ADV for terminal a and c phases to ground fault.

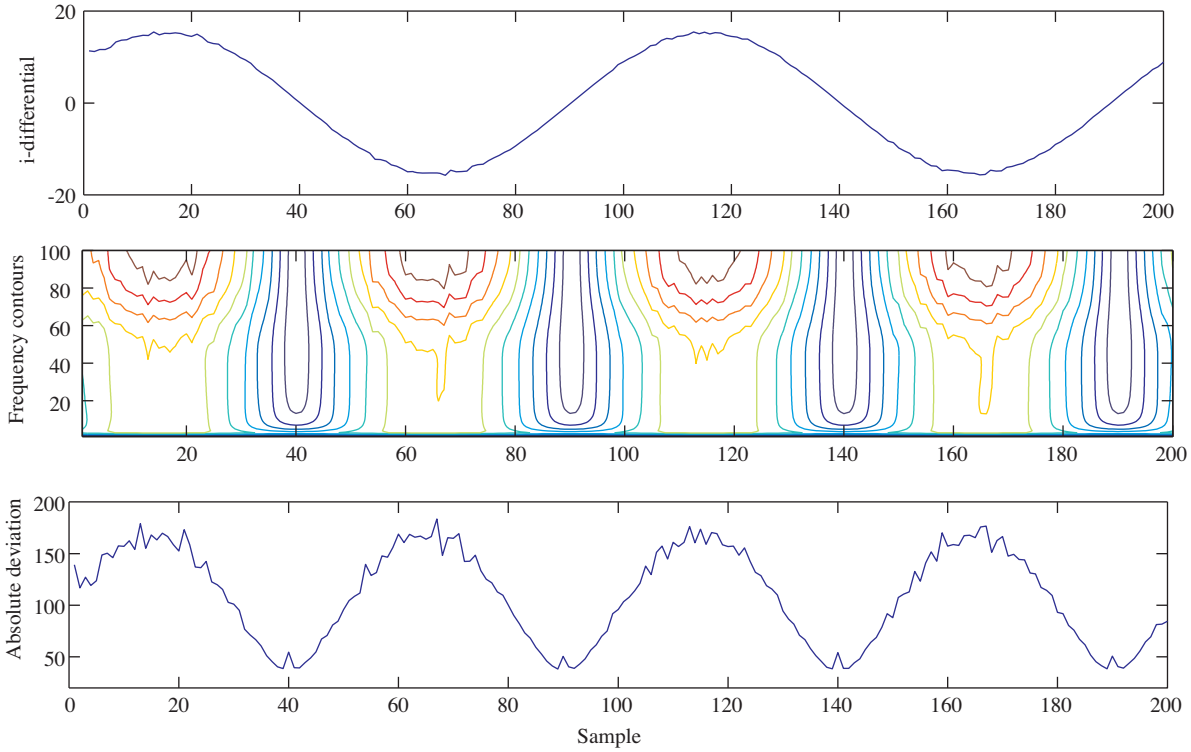

Figure 16. Differntial current with SNR = 20 dB, S-contours, and ADV for internal turn-to-turn fault between turns 294 and 343.

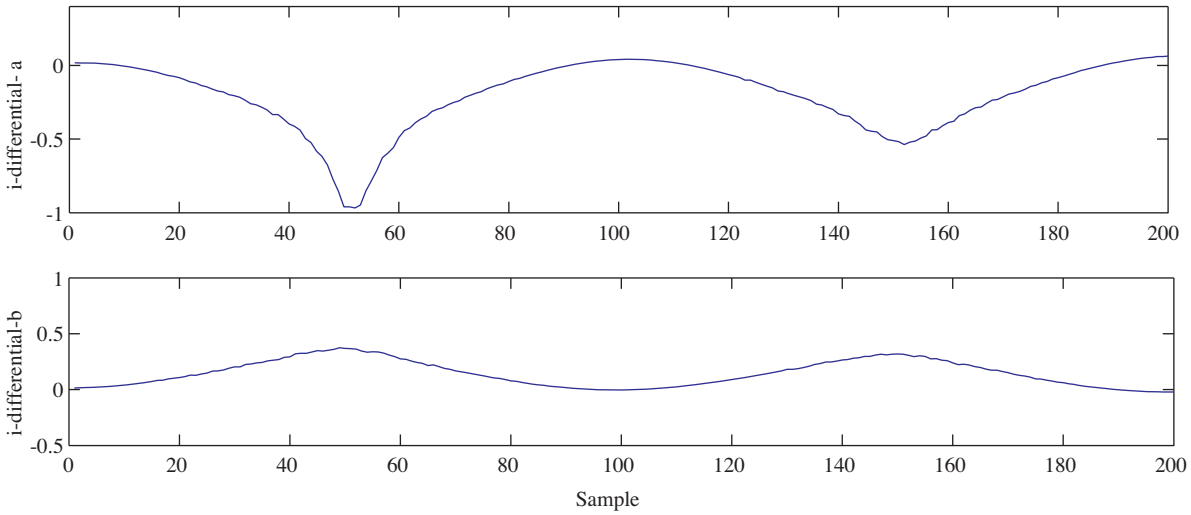

Figure 17. Differntial current with SNR = 20 dB for external abg fault in middle of transmission line; secondary CTs have been saturated.

denote phase B of the primary side-to-ground fault, phase a and c of the secondary side-to-ground fault, and the phase a to c fault, respectively. The results for noisy conditions are also included in the Table. In the presented cases, the SAD values are between 4393.2 and 9105.8 in the inrush current cases. However, the SAD values in the cases of internal faults during normal operation or transformer energization are between 10,054.7

Table. Simulation results.

Disturbance	Phase A angle at fault instance	Fault resistance	Phase	Without noise	With noise	% error
				SAD	SAD	
Inrush with load	0	-	A	5306	5319.9	0.262
			B	4713.3	4709.8	0.074
			C	8781.4	8805.6	0.274
Inrush with load	150	-	A	7888.8	7909	0.256
			B	4393.2	4400.2	0.158
			C	7269.2	7265.1	0.056
Inrush, no load	45	-	A	4869.9	4872.3	0.048
			B	9105.8	9119.6	0.151
			C	6879.7	6884.2	0.066
Inrush, no load	90	-	A	8168.2	8181.9	0.167
			B	8220	8231.1	0.135
			C	4874.7	4876	0.026
Inrush and internal turn 294-Bg	135	2	A	8319	8353	0.406
			B	44,161.1	44,249.5	0.2
			C	50,234.8	50,282.5	0.095
Inrush and internal turn 343-Bg	145	3	A	7803.4	7786.9	0.212
			B	42,362.7	42,348.5	0.034
			C	48,440.3	48,421.2	0.039
Inrush and internal turns 294 to 343-Bg	0	3	A	5138.9	5132.8	0.118
			B	10,485.1	10,472.5	0.12
			C	15,217.1	15,213.7	0.023
Internal turn 294-Bg	90	3	A	48.4	48.5	0.143
			B	36,214.7	36,115.5	0.275
			C	36,260	36,247.4	0.035
Internal turn 294-Bg	0	6	A	48.5	48.5	0.04
			B	20,262.3	20,235.5	0.132
			C	20,310	20,293.7	0.08
Internal turn 343-Bg	30	5	A	48.4	48.5	0.177
			B	31,155.4	31,176.2	0.067
			C	31,202.3	31,242.5	0.129
Internal turn 343-Bg	0	3	A	48.4	48.4	0.041
			B	45,594.6	45,626.6	0.07
			C	45,638	45,695	0.125
Internal turns 294-343-Bg	90	2	A	48.9	48.9	0.007
			B	13860.6	13883.5	0.165
			C	13908.7	13905.3	0.024
Internal turns 294-343-Bg	25	3	A	48.4	48.4	0.03
			B	10054.7	10071.7	0.169
			C	10103.7	10113.8	0.1
Terminal fault acg	0	4	A	22382.6	22364	0.083
			B	47.8	47.9	0.242
			C	23053.3	23042.5	0.047
Terminal fault ac	30	0	A	34460.3	34432.5	0.081
			B	48.7	48.7	0.002
			C	34452	34447	0.015

and 50,234.8 (in faulty phases). It is found that the SAD values are less influenced by noise. Furthermore, the SAD values in the internal fault and inrush current cases do not have any overlap, even for the cases where a fault occurred in only 5% of the winding. Thus, it is easy to discriminate between fault and inrush currents, even in noisy environments. Since secondary windings of the power transformer and primary CTs are connected as delta, a fault in phase B results in high values of the SAD in phase b and c.

6. Comparison between S-transform and wavelet transform

In order to compare the S-transform with the wavelet transform, the DWT simulation has been implemented. The Daubechies 2 (db2) has been chosen as the mother wavelet and the differential current signals are decomposed up to the third level. The sampling frequency is 5 kHz. In the case of the inrush current (shown in Figure 6), the differential current details up to the third level are illustrated in Figure 18. The first detail, in which the spikes are more obvious, is selected for analysis. It can be seen that the spikes continue during several cycles and there is a consistent time interval between them, and so the spikes occur consistently. Figure 19 shows the DWT for the turn-to-earth fault at turn 294 of phase B in the primary winding (illustrated in Figure 7). A fault occurs at t =6 ms. The spikes occur at the fault instance and they decay quickly to near 0 within half a cycle in the first detail. In order to investigate the performance of the wavelet transform in noisy environments, random noise with a SNR of up to 20 dB has been added to the differential current signals of the above-mentioned cases. The results are shown in Figures 20 and 21. It is found that the noise has an obvious effect on the wavelet transform and it is difficult to distinguish between the internal fault and the inrush current. Hence, the spike-shaped waveforms affect the wavelet-based method (such as in [8], [14], and [32]) in a noisy environment.

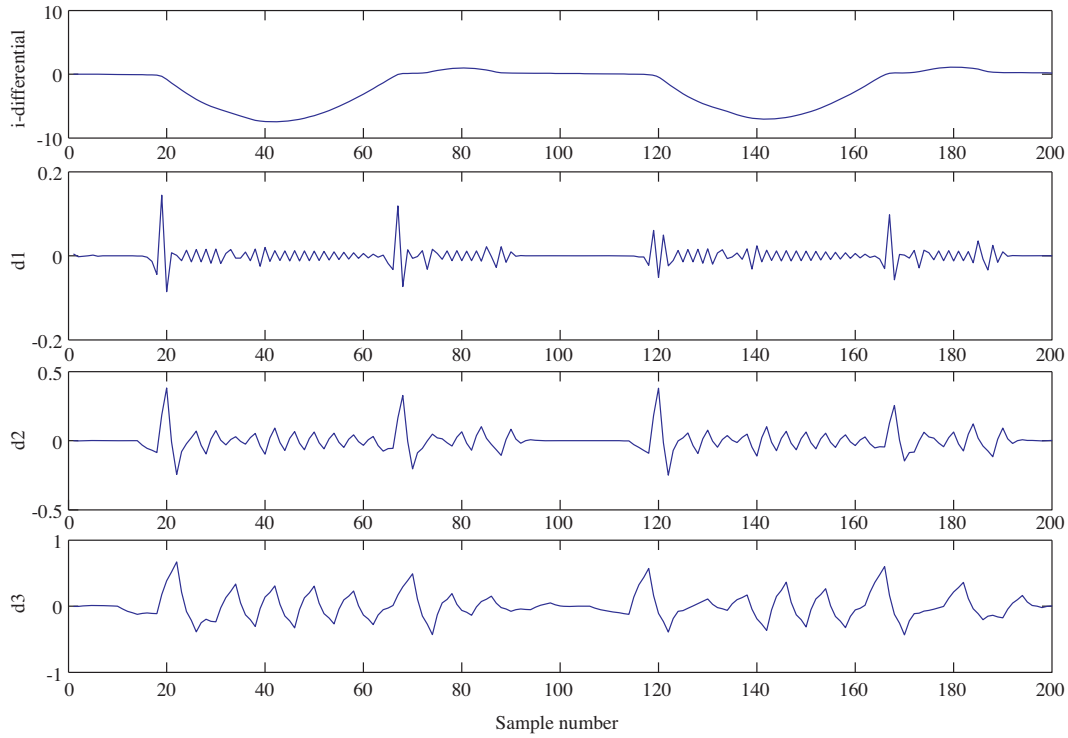

Figure 18. Differntial current and details up to third level for inrush current.

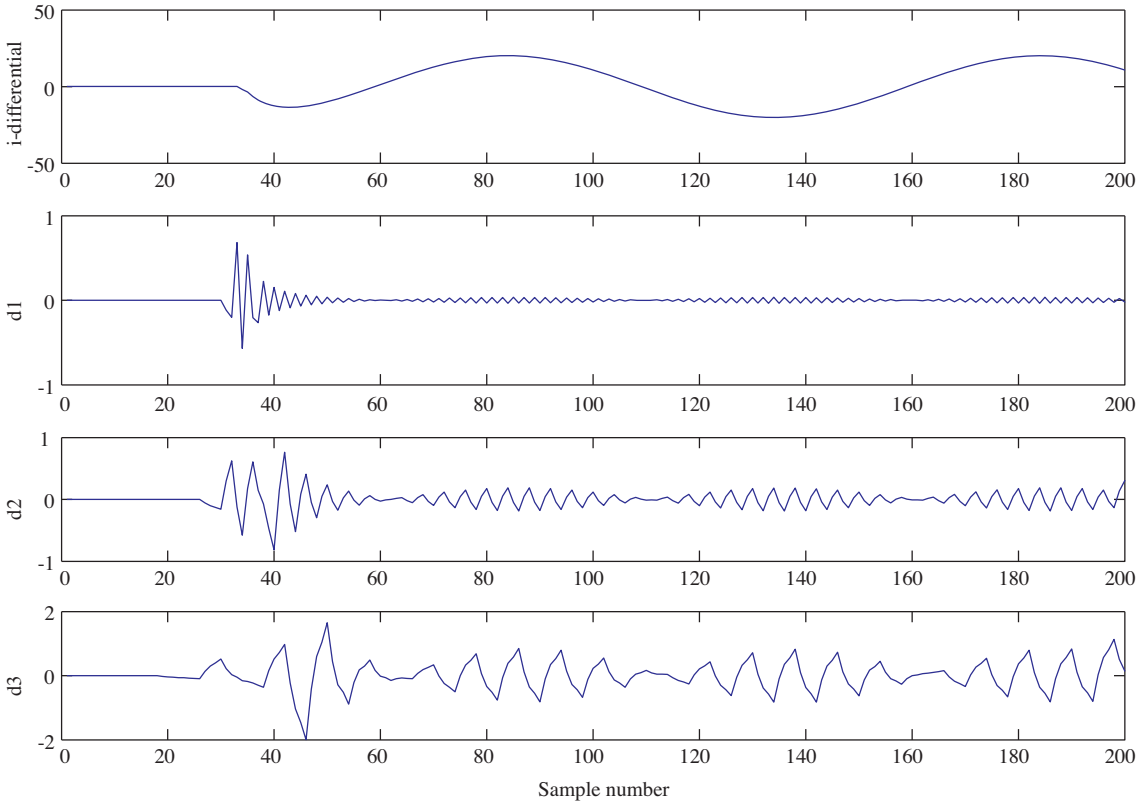

Figure 19. Differential current and details up to third level for internal turn-to-earth fault at turn 294.

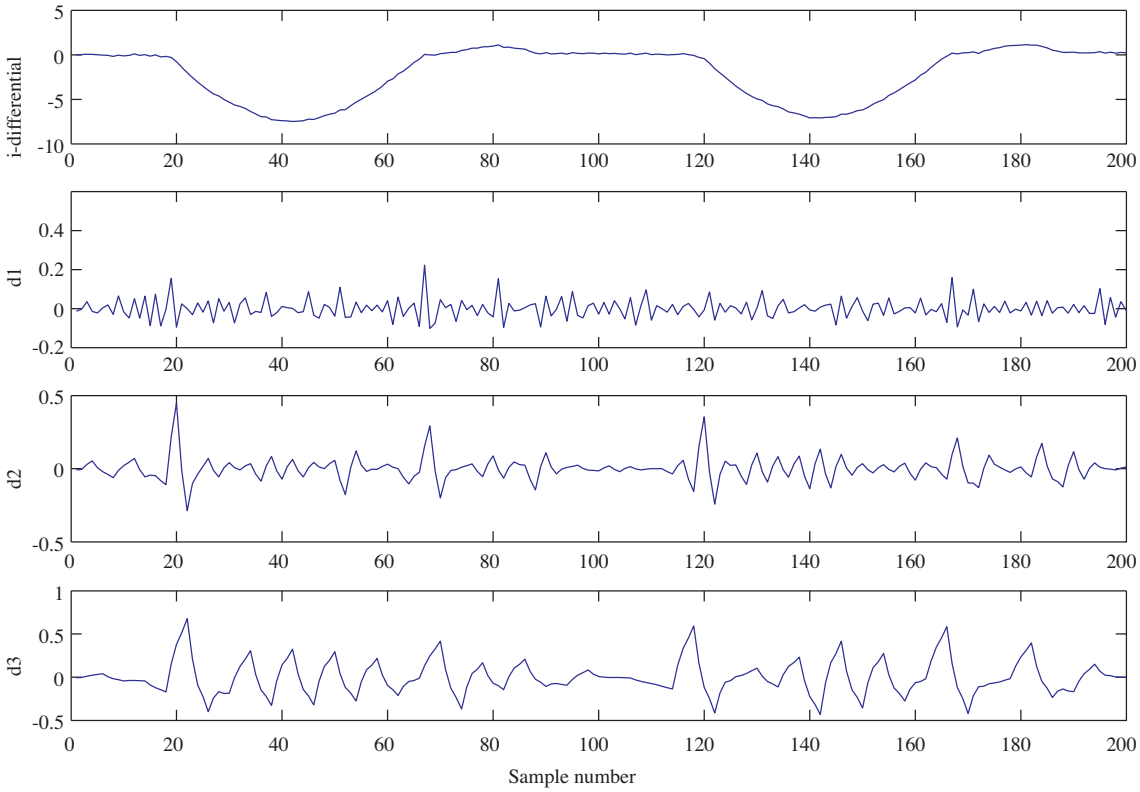

Figure 20. Differential current with SNR = 20 dB and details up to third level for inrush current.

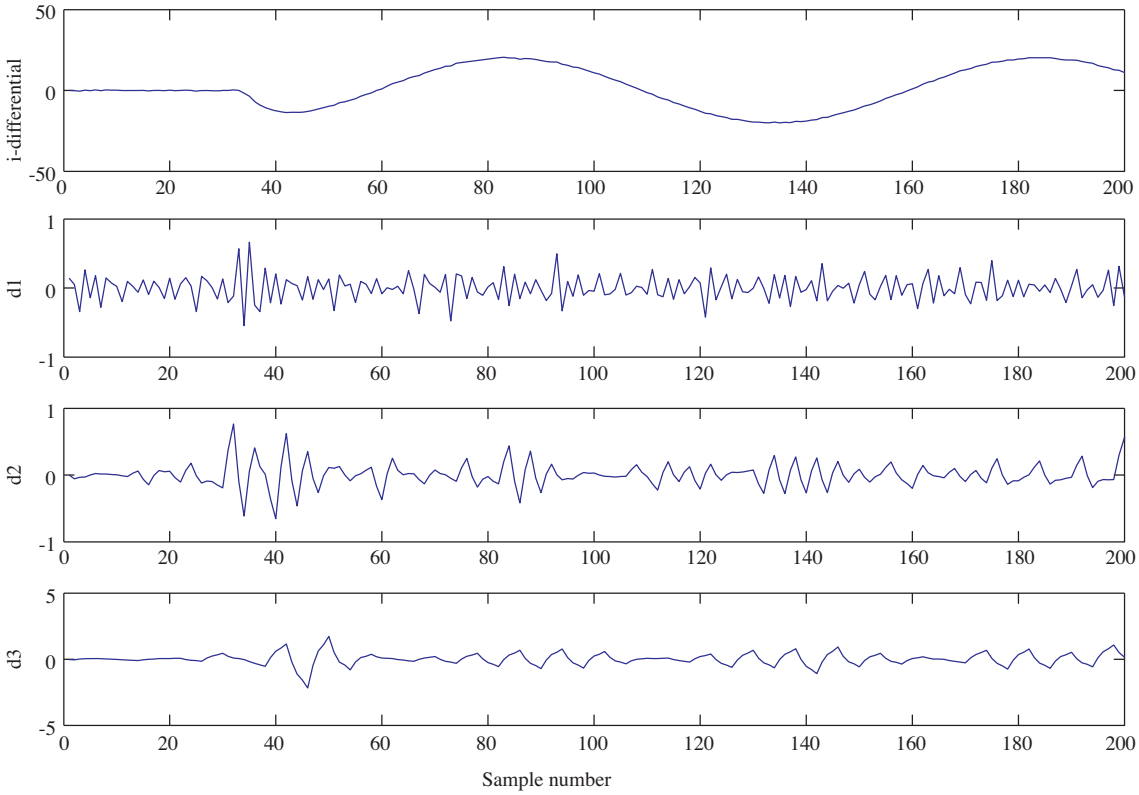

Figure 21. Differntial current with SNR = 20 dB and details up to third level for internal turn-to-earth fault at turn 294.

7. Conclusion

In this paper, a new 2-stage algorithm for distinguishing the most important types of transients of power transformers has been suggested. Using this method, the external fault and internal disturbances can be distinguished in the first stage. Next, in the second stage, the inrush current or the internal fault can be detected and discriminated in internal disturbances. An index, named SAD, has been proposed and calculated using the absolute deviation of the S-matrix. According to simulation results, it is shown that different faults can be detected by comparison of the SAD values of the faulty phases with a boundary value. To study the effectiveness of the proposed algorithm, it has been implemented in a MATLAB environment linked with EMTP software. In order to compare the performance of the S-transform and the wavelet transform, a wavelet-based method has also been implemented. Several cases have been considered to study the performance of both methods with and without noise. According to simulation results, it can be seen that the wavelet-based method has been easily influenced by noise; however, the suggested algorithm can truly discriminate between faulty and unfaulty currents, even in cases of CT saturation, ratio mismatch, and noisy conditions.

References

[1] T.S. Sidhu, M.S. Sachdev, "On line identification of magnetizing inrush and internal faults in three-phase transformers", IEEE Transactions on Power Delivery, Vol. 7, pp. 1885–1890, 1992.

[2] B. Kasztenny, A. Kulidjian, "An improved transformer inrush restraint algorithm increases security while maintaining fault response performance", 53rd Annual Conference for Protective Relay Engineers, pp. 2–27, 2000.

[3] H. Zhang, P. Liu, O.P. Malik, "A new scheme for inrush identification in transformer protection", Electric Power System Research, Vol. 63, pp. 81–86, 2002.

[4] M.A. Rahman, B. Jeyasurya, "A state-of-the-art review of transformer protection algorithms", IEEE Transactions on Power Delivery, Vol. 3, pp. 534–544, 1988.

[5] P.L. Mao, R.K. Aggarwal, "A novel approach to the classification of the transient phenomena in power transformers using combined wavelet transform and neural network", IEEE Transactions on Power Delivery, Vol. 16, pp. 654–660, 2001.

[6] S.A. Saleh, M.A. Rahman, "Modeling and protection of a three phase power transformer using wavelet packet transform", IEEE Transactions on Power Delivery, Vol. 20, pp. 1273–1282, 2005.

[7] M.M. Eissa, "A novel digital directional transformer protection technique based on wavelet packet", IEEE Transactions on Power Delivery, Vol. 20, pp. 1830–1836, 2005.

[8] M. Kitayama, "Wavelet-based fast discrimination of transformer magnetizing inrush current", Electrical Engineering in Japan, Vol. 158, pp. 19–28, 2007.

[9] A.A.H. Eldin, M.A. Refaey, "A novel algorithm for discrimination between inrush current and internal faults in power transformer differential protection based on discrete wavelet transform", Electric Power Systems Research, Vol. 81, pp. 19–24, 2011.

[10] E.M. Tag Eldin, "A new algorithm for the classification of different transient phenomena in power transformers combining wavelet transforms and fuzzy logic", IEEE 46th Midwest Symposium on Circuits and Systems, Vol. 3, pp. 116–1121, 2003.

[11] N. Hong Viet, N. Tuan Dung, "New approach for classifying transient phenomena in power transformer using discrete wavelet transforms (DWT) and fuzzy logic", International Symposium on Electrical and Electronics Engineering, pp. 261–265, 2007.

[12] M. Geethanjali, S.M.R. Slochanal, R. Bhavani, "A novel approach for power transformer protection based upon combined wavelet transform and neural networks (WNN)", 7th International Power Engineering Conference, pp. 1–6, 2005.

[13] S. Jazebi, B. Vahidi, S.H. Hosseinian, J. Faiz, "Magnetizing inrush current identification using wavelet based gaussian mixture models", Simulation Modelling Practice and Theory, Vol. 17, pp. 991–1010, 2009.

[14] H.K. Kargar, M. Jabbari, S. Golmohammad Zadeh, "Inrush current identification based on wavelet transform and correlation factors", 6th International Conference on Electrical Engineering/Electronics, Computer, Telecommunications and Information Technology, Vol. 1, pp. 50–53, 2009.

[15] S. Jazebi, B. Vahidi, M. Jannati, "A novel application of wavelet based SVM to transient phenomena identification of power transformers", Energy Conversion and Management, Vol. 52, pp. 1354–1363, 2011.

[16] S. Subramanian, M. Badrilal, J. Henry, "Wavelet packet transform and support vector machine based discrimination of power transformer inrush current from internal fault currents", Modern Applied Science, Vol. 4, pp. 67–82, 2010.

[17] Q. Zhang, S. Jiao, S. Wang, "Identification inrush current and internal faults of transformer based on Hyperbolic S-transform", 4th IEEE International Conference on Industrial Electronics and Applications, pp. 258–263, 2009.

[18] B.K. Panigrahi, S.R Samantaray, P.K. Dash, G. Panda, "Discrimination between inrush current and internal faults using pattern recognition approach", International Conference on Power Electronics, Drives and Energy Systems, pp. 1–5, 2006.

[19] S. Jia, S. Wang, G. Zheng, "A new approach to identify inrush current based on generalized S-transform", International Conference on Electrical Machines and Systems, pp. 4317–4322, 2008.

[20] S. Sendilkumar, B.L. Mathur, J. Henry, "A new technique to classify transient events in power transformer differential protection using S-transform", 3rd International Conference on Power Systems, pp. 1–6, 2009.

[21] S.R. Samantaray, B.K. Panigrahi, P.K. Dash, G. Panda, "Power transformer protection using S-transform with complex window and pattern recognition approach", IET Generation, Transmission & Distribution, Vol. 1, pp. 278–286, 2007.

[22] G. Mokryani, M.R. Haghifam, H. Latafat, P. Aliparast, A. Abdollahy, "Detection of inrush current using S-transform and probabilistic neural network", IEEE/PES Transmission and Distribution Conference and Exposition, pp. 1–6, 2010.

[23] R.G. Stockwell, L. Mansinha, R.P. Lowe, "Localization of the complex spectrum: the S transform", IEEE Transactions on Signal Processing, Vol. 44, pp. 998–1001, 1996.

[24] M.O. Oliveira, R.H. Salim, A.S. Bretas, "Differential protection of three-phase transformers using wavelet transforms", IEEE/PES Transmission and Distribution Conference and Exposition, pp. 1–6, 2008.

[25] S.H. Horowitz, A.G. Phadke, Power System Relaying, 3rd ed., New York, Wiley, 1988.

[26] S.P. Valsan, K.S. Swarup, "Wavelet based transformer protection using high frequency power directional signals", Electric Power Systems Research, Vol. 78, pp. 547–558, 2008.

[27] P. Bastard, P. Bertrand, M. Meunier, "A transformer model for winding fault studies", IEEE Transactions on Power Delivery, Vol. 9, pp. 690–699, 1994.

[28] M. Kezunovic, Y. Guo, "Modeling and simulation of the power transform faults and related protective relay behavior", IEEE Transactions on Power Delivery, Vol. 15, pp. 44–50, 2000.

[29] R.M. Rifaat, "Considerations in applying EMTP to evaluate current transformer performance under transient and high current fault conditions", International Conference on Power Systems Transients, 2005.

[30] S. Dennetière, J. Mahseredjian, M. Martinez, M. Rioual, A. Xémard, P. Bastard, "On the implementation of a hysteretic reactor model in EMTP", Proceedings of the 5th International Conference on Power Systems Transients, pp. 1–5, 2003.

[31] ANSI/IEEE, Requirements for Instrument Transformers, ANSI/IEEE Standard C57.13, New York, 1978.

[32] J. Faiz, S. Lotfi-Fard, "A novel wavelet-based algorithm for discrimination of internal faults from magnetizing inrush currents in power transformers", IEEE Transactions on Power Delivery, Vol. 21, pp. 1989–1996, 2006.